Implementation of the modified Cam Clay model in MFront/OpenGeoSys

Christian Silbermann, Thomas Nagel

July 27, 2021

This report describes the implementation of the basic modified Cambridge (Cam) clay material model for small strains in the open-source multi-field software *OpenGeoSys*. For this, the set of constitutive equations is outlined and summarized. For the sake of simplicity, the elastic material parameters are kept constant. Therefore, the model is called *basic* modified Cam clay model. An implicit numerical solution scheme is presented with additional options of refinement and stabilization. Based on the interface *MFront*, the implementation is outlined briefly. Then, numerical studies are presented for a single integration point using *MFront mtest*, and eventually for meshes consisting of one or multiple finite elements using *OpenGeoSys*.

1 Introduction

The Cambridge (Cam) clay model describes the stress-dependent deformation behaviour of cohesive soils. Thereby, effects like

1. elasto-plastic deformation,
2. irreversible (plastic) pore compaction,
3. hardening and softening,
4. consolidation,
5. different loading and unloading stiffness

can be considered. Typical applications for the Cam clay model are the calculation of soil strata, for example in geomechanical simulations. The goal of this technical report is a consistent and clear presentation of the basic modified Cam clay model ready for implementation and practical use in continuum mechanical simulations using FEM. Here, the material model interface *MFront* is used. For the sake of compactness, a symbolic tensor notation is used where the number of underscores indicates the order of the tensor object.

2 Constitutive equations

2.1 Preliminaries

In the small-strain setting there is an additive split of the linear strain tensor reading

$$\underline{\underline{\varepsilon}} = \underline{\underline{\varepsilon}}_{\mathrm{e}} + \underline{\underline{\varepsilon}}_{\mathrm{p}} \ . \tag{1}$$

The generalized Hooke's law relates elastic strains with stresses as

$$\underline{\underline{\sigma}} = \underline{\underline{\underline{\underline{D}}}} \cdot\cdot \ \underline{\underline{\varepsilon}}_{\mathrm{e}} \ . \tag{2}$$

Splitting the stress tensor[1] with respect to deviatoric and volumetric parts yields

$$\underline{\underline{\sigma}} = \underline{\underline{\sigma}}^{\mathrm{D}} + \frac{1}{3} I_1(\underline{\underline{\sigma}}) \underline{\underline{I}} \ . \tag{3}$$

Therewith, the von-Mises stress and the hydrostatic pressure is defined as

$$q \coloneqq \sqrt{\tfrac{3}{2} \ \underline{\underline{\sigma}}^{\mathrm{D}} \cdot\cdot \ \underline{\underline{\sigma}}^{\mathrm{D}}} \quad , \quad p \coloneqq -\frac{1}{3} I_1(\underline{\underline{\sigma}}) \ . \tag{4}$$

Consequently, positive values of p represent a pressure whereas negative values represent hydrostatic tension, as expected. With this, the stress tensor split reads $\underline{\underline{\sigma}} = \underline{\underline{\sigma}}^{\mathrm{D}} - p\underline{\underline{I}}$. Later the following derivatives will be required:

$$\frac{\partial q}{\partial \underline{\underline{\sigma}}} = \frac{3}{2} \ \frac{\underline{\underline{\sigma}}^{\mathrm{D}}}{q} \quad , \quad \frac{\partial p}{\partial \underline{\underline{\sigma}}} = -\frac{1}{3} \ \underline{\underline{I}} \ . \tag{5}$$

Dealing with porous media there is a kinematic relation between porosity and volumetric strain. Let the total volume of an REV be divided into a pore volume and the solid volume:

$$V = V_{\mathrm{S}} + V_{\mathrm{P}} \ . \tag{6}$$

Now, the porosity is defined as the pore volume fraction, i. e. $\phi = V_{\mathrm{P}}/V$. Evaluating the mass balance equation of the porous solid yields the porosity evolution in the form

$$\dot{\phi} - \phi \, \mathrm{div}(\dot{\underline{u}}) = \mathrm{tr}(\dot{\underline{\underline{\varepsilon}}}) \ . \tag{7}$$

Exploiting $\mathrm{div}(\dot{\underline{u}}) \equiv \mathrm{tr}(\dot{\underline{\underline{\varepsilon}}})$ and separating the variables, this differential equation can be solved in a straightforward manner (cf. App.). If the elastic volume changes are small compared to the plastic ones, the porosity (evolution) can be calculated from $\varepsilon_{\mathrm{p}}^{\mathrm{V}}$ only. Instead of the porosity ϕ, the pore number $e = V_{\mathrm{P}}/V_{\mathrm{S}}$ can equally be used with the relations

$$e = \frac{\phi}{1-\phi} \quad \text{with} \quad 1 + e = (1-\phi)^{-1} \ . \tag{8}$$

[1] In soil mechanics, this would be the effective stress tensor. As the context is clear here, we refrain from writing $\underline{\underline{\sigma}}'$. Note also that a mechanical sign convention is used in contrast to the soil mechanical concepts.

2.2 System of equations

The following set of equations fully describes the basic modified Cam clay model. Elasticity is

$$\underline{\underline{\sigma}} = \underline{\underline{\underline{\underline{D}}}} \cdot\cdot \left(\underline{\underline{\varepsilon}} - \underline{\underline{\varepsilon}}_{\mathrm{p}}\right) \ . \tag{9}$$

Then, the *modified* Cam clay yield function with the parameters M and $p_{\mathrm{c}}(e)$ is given by

$$f \coloneqq q^2 + Mp(p - p_{\mathrm{c}}) \leq 0 \ . \tag{10}$$

An associated flow rule (normality rule) is used to obtain the plastic flow as[2]

$$\dot{\underline{\underline{\varepsilon}}}_{\mathrm{p}} = \dot{\Lambda}_{\mathrm{p}} \ \underline{\underline{n}} \quad \text{with} \quad \underline{\underline{n}} = \frac{\underline{\underline{m}}}{\|\underline{\underline{m}}\|} \quad , \quad \underline{\underline{m}} = \frac{\partial f}{\partial \underline{\underline{\sigma}}} \ . \tag{11}$$

where $\dot{\Lambda}_{\mathrm{p}}$ denotes the plastic multiplier such that $\mathrm{d}\Lambda_{\mathrm{p}}$ is the plastic increment and $\underline{\underline{n}}$ gives the direction of the plastic flow. The plastic volume change rate is obtained from

$$\dot{\varepsilon}_{\mathrm{p}}^{\mathrm{V}} = \mathrm{tr}(\dot{\underline{\underline{\varepsilon}}}_{\mathrm{p}}) = \dot{\Lambda}_{\mathrm{p}} \, \mathrm{tr}(\underline{\underline{n}}) \ . \tag{12}$$

The so-called pre-consolidation pressure p_{c} represents the yield stress under isotropic compression and evolves as

$$\dot{p}_{\mathrm{c}} = \text{-}\dot{\varepsilon}_{\mathrm{p}}^{\mathrm{V}} \vartheta(e) \ p_{\mathrm{c}} \quad \text{with} \quad p_{\mathrm{c}}\big|_{t=0} = p_{\mathrm{c0}} \ . \tag{13}$$

This way, the pre-consolidation pressure increases in case of plastic compaction, i. e. $\dot{\varepsilon}_{\mathrm{p}}^{\mathrm{V}} < 0$. Moreover, the pre-consolidation pressure remains constant during purely elastic loading. Furthermore, the parameter ϑ depends on the pore number e or the porosity ϕ, respectively:

$$\vartheta(e) = \frac{1+e}{\lambda - \kappa} \overset{(8)}{=} \frac{1}{(\lambda - \kappa)(1 - \phi)} = \vartheta(\phi) \ , \tag{14}$$

where the material constants λ, κ represent the slope of the virgin normal consolidation line and the normal swelling line, respectively (with $\lambda > \kappa$), in a semi-logarithmic $(1 + e) - \ln p$ plot. This gives

$$\dot{p}_{\mathrm{c}} = -\dot{\varepsilon}_{\mathrm{p}}^{\mathrm{V}} \left(\frac{1+e}{\lambda - \kappa}\right) \ p_{\mathrm{c}} \ . \tag{15}$$

With the porosity evolution given by formula (7), the system of constitutive equations for the modified Cam clay model is closed. This way, all the basic effects $1. - 5.$ are captured.

In order to refine effect 5., namely load-path dependent elastic stiffness, an evolution equation for the hydrostatic pressure and the elastic volumetric strain, respectively, has to be added [6]:

$$\dot{p} = -\dot{\varepsilon}_{\mathrm{e}}^{\mathrm{V}} \left(\frac{1+e}{\kappa}\right) \ p \ . \tag{16}$$

[2] Note that we deviate here from the classical form by means of normalizing the yield function gradient in stress space. This was done in an effort to maintain consistency in the units, as the MCC yield function has dimensions of stress squared in contrast to the usual units of stress.

As a consequence, the compression modulus becomes load-path-dependent, too. Then, care must be taken that the constitutive equations are still thermodynamically consistent [5]. I also seems counter-intuitive that the bulk modulus should increase with the pore number. For these reasons and for the sake of simplicity, linear elasticity is used here. This means instead of (16) holds

$$\dot{p} = -\dot{\varepsilon}_{\mathrm{e}}^{\mathrm{V}} \; K \; , \tag{17}$$

which is automatically fulfilled applying linear elasticity (9) with a constant bulk modulus K.

3 Numerical solution

3.1 Total implicit solution scheme

For a time integration, the total values at the next instant of time are calculated from the current values and the increments, i. e.

$$\underline{\underline{\varepsilon}}_{\mathrm{e}} \coloneqq {}^{k+1}\underline{\underline{\varepsilon}}_{\mathrm{e}} = {}^{k}\underline{\underline{\varepsilon}}_{\mathrm{e}} + \theta \Delta \underline{\underline{\varepsilon}}_{\mathrm{e}} \; , \tag{18a}$$

$$\Lambda_p \coloneqq {}^{k+1}\Lambda_p = {}^{k}\Lambda_p + \theta \Delta \Lambda_p \; , \tag{18b}$$

$$p_{\mathrm{c}} \coloneqq {}^{k+1}p_{\mathrm{c}} = {}^{k}p_{\mathrm{c}} + \theta \Delta p_{\mathrm{c}} \; , \tag{18c}$$

$$\phi \coloneqq {}^{k+1}\phi = {}^{k}\phi + \theta \Delta \phi \; , \tag{18d}$$

The discretized incremental evolution equation now read

$$\Delta \underline{\underline{\varepsilon}}_{\mathrm{p}} = \Delta \Lambda_{\mathrm{p}} \; \underline{\underline{n}} \; , \tag{19a}$$

$$\Delta \varepsilon_{\mathrm{p}}^{\mathrm{V}} = \Delta \Lambda_{\mathrm{p}} \, \mathrm{tr}(\underline{\underline{n}}) \; , \tag{19b}$$

$$\Delta p_{\mathrm{c}} = -\Delta \varepsilon_{\mathrm{p}}^{\mathrm{V}} \vartheta(e) \; p_{\mathrm{c}} \; , \tag{19c}$$

$$\Delta \phi = (1 - \phi) \Delta \varepsilon^{\mathrm{V}} \; . \tag{19d}$$

With this, the discretized set of equations has the form

$$\underline{\underline{f}}_{\varepsilon_{\mathrm{e}}} = \Delta \underline{\underline{\varepsilon}}_{\mathrm{e}} + \Delta \Lambda_p \; \underline{\underline{n}} - \Delta \underline{\underline{\varepsilon}} = \underline{\underline{0}} \; , \tag{20a}$$

$$f_{\Lambda_p} = q^2 + M^2 (p^2 - p \, p_{\mathrm{c}}) = 0 \; , \tag{20b}$$

$$f_{p_{\mathrm{c}}} = \Delta p_{\mathrm{c}} + \Delta \varepsilon_{\mathrm{p}}^{\mathrm{V}} \vartheta(\phi) \; p_{\mathrm{c}} = 0 \; , \tag{20c}$$

$$f_{\phi} = \Delta \phi - (1 - \phi) \Delta \varepsilon^{\mathrm{V}} = 0 \; , \tag{20d}$$

where the total values are the values at the next instant of time, meaning $q = {}^{k+1}q, p = {}^{k+1}p$. For the partial derivatives the functional dependencies are required. They read

$$\underline{\underline{f}}_{\varepsilon_{\mathrm{e}}} = \underline{\underline{f}}_{\varepsilon_{\mathrm{e}}} (\Delta \underline{\underline{\varepsilon}}_{\mathrm{e}}, \Delta \Lambda_p, \Delta p_{\mathrm{c}}) \; , \tag{21a}$$

$$f_{\Lambda_p} = f_{\Lambda_p} (\Delta \underline{\underline{\varepsilon}}_{\mathrm{e}}, \Delta p_{\mathrm{c}}) \; , \tag{21b}$$

$$f_{p_{\mathrm{c}}} = f_{p_{\mathrm{c}}} (\Delta \underline{\underline{\varepsilon}}_{\mathrm{e}}, \Delta \Lambda_p, \Delta p_{\mathrm{c}}, \Delta \phi) \; , \tag{21c}$$

$$f_{\phi} = f_{\phi} (\Delta \phi) \; , \tag{21d}$$

where it was taken into account, that $q(\underline{\underline{\sigma}}), p(\underline{\underline{\sigma}})$ and $\underline{\underline{\sigma}}(\Delta\underline{\underline{\varepsilon}}_{\mathrm{e}})$ and $\underline{\underline{n}}(q,p,p_{\mathrm{c}})$ and $\Delta\varepsilon_{\mathrm{p}}^{\mathrm{V}}(\Delta\Lambda_p,\underline{\underline{n}})$.

For the solution of the incremental set of equations (20) with the Newton-Raphson method the partial derivatives with respect to the increments of the unknowns are required. They read

$$\frac{\partial \underline{\underline{f}}_{\varepsilon_{\mathrm{e}}}}{\partial \Delta\underline{\underline{\varepsilon}}_{\mathrm{e}}} = \underline{\underline{\underline{\underline{I}}}} + \Delta\Lambda_p \frac{\partial \underline{\underline{n}}}{\partial \Delta\underline{\underline{\varepsilon}}_{\mathrm{e}}} \quad \text{with} \quad \underline{\underline{\underline{\underline{I}}}} = \underline{e}_a \otimes \underline{e}_b \otimes \underline{e}_a \otimes \underline{e}_b \ , \tag{22a}$$

$$\frac{\partial \underline{\underline{f}}_{\varepsilon_{\mathrm{e}}}}{\partial \Delta\Lambda_p} = \underline{\underline{n}} \ , \tag{22b}$$

$$\frac{\partial \underline{\underline{f}}_{\varepsilon_{\mathrm{e}}}}{\partial \Delta p_{\mathrm{c}}} = \Delta\Lambda_p \ \frac{\partial \underline{\underline{n}}}{\partial \Delta p_{\mathrm{c}}}, \tag{22c}$$

$$\frac{\partial f_{\Lambda_p}}{\partial \Delta\underline{\underline{\varepsilon}}_{\mathrm{e}}} = \frac{\partial f_{\Lambda_p}}{\partial \underline{\underline{\sigma}}} : \frac{\partial \underline{\underline{\sigma}}}{\partial \underline{\underline{\varepsilon}}_{\mathrm{e}}} : \frac{\partial \underline{\underline{\varepsilon}}_{\mathrm{e}}}{\partial \Delta\underline{\underline{\varepsilon}}_{\mathrm{e}}} = \underline{\underline{m}} : \underline{\underline{\underline{\underline{D}}}} \ \theta \ , \tag{22d}$$

$$\frac{\partial f_{\Lambda_p}}{\partial \Delta p_{\mathrm{c}}} = \frac{f_{\Lambda_p}}{\partial p_{\mathrm{c}}} \ \frac{\partial p_{\mathrm{c}}}{\partial \Delta p_{\mathrm{c}}} = -pM^2 \, \theta \ , \tag{22e}$$

$$\frac{\partial f_{p_{\mathrm{c}}}}{\partial \Delta\underline{\underline{\varepsilon}}_{\mathrm{e}}} = \frac{\partial f_{p_{\mathrm{c}}}}{\partial \underline{\underline{n}}} : \frac{\partial \underline{\underline{n}}}{\partial \Delta\underline{\underline{\varepsilon}}_{\mathrm{e}}} \ , \tag{22f}$$

$$\frac{\partial f_{p_{\mathrm{c}}}}{\partial \Delta\Lambda_p} = \frac{\partial f_{p_{\mathrm{c}}}}{\partial \Delta\varepsilon_{\mathrm{p}}^{\mathrm{V}}} \ \frac{\partial \Delta\varepsilon_{\mathrm{p}}^{\mathrm{V}}}{\partial \Lambda_p} = \vartheta p_{\mathrm{c}} \, \mathrm{tr}(\underline{\underline{n}}) \ , \tag{22g}$$

$$\frac{\partial f_{p_{\mathrm{c}}}}{\partial \Delta p_{\mathrm{c}}} = 1 + \vartheta \Delta\varepsilon_{\mathrm{p}}^{\mathrm{V}} \theta + \frac{\partial f_{p_{\mathrm{c}}}}{\partial \underline{\underline{n}}} : \frac{\partial \underline{\underline{n}}}{\partial \Delta p_{\mathrm{c}}} \ , \tag{22h}$$

$$\frac{\partial f_{p_{\mathrm{c}}}}{\partial \Delta\phi} = \Delta\varepsilon_{\mathrm{p}}^{\mathrm{V}} p_{\mathrm{c}} \frac{\partial \vartheta(\phi)}{\partial \phi} \ \frac{\partial \phi}{\partial \Delta\phi} = \frac{\Delta\varepsilon_{\mathrm{p}}^{\mathrm{V}} p_{\mathrm{c}} \, \theta}{(\lambda-\kappa)(1-\phi)^2} \ , = \frac{\Delta\varepsilon_{\mathrm{p}}^{\mathrm{V}} p_{\mathrm{c}} \, \vartheta \, \theta}{(1-\phi)} \ , \tag{22i}$$

$$\frac{\partial f_{\phi}}{\partial \Delta\phi} = 1 + \theta \Delta\varepsilon^{\mathrm{V}} \ . \tag{22j}$$

All other partial derivatives vanish according to the (missing) dependencies (21). Using the normalized flow direction $\underline{\underline{n}}$, the derivatives with respect to some variable X can be obtained with the following rule:

$$\frac{\partial \underline{\underline{n}}}{\partial X} = \frac{1}{m} \left\{ \frac{\partial \underline{\underline{m}}}{\partial X} - \frac{1}{2} \, \underline{\underline{n}} \otimes \frac{1}{m} \frac{\partial m^2}{\partial X} \right\} \quad \text{with} \quad m = \|\underline{\underline{m}}\| \ . \tag{23}$$

Now, the missing expressions in overview (22) can be calculated as

$$\underline{\underline{m}} = \frac{\partial f}{\partial \underline{\underline{\sigma}}} = \frac{\partial f}{\partial q}\frac{\partial q}{\partial \underline{\underline{\sigma}}} + \frac{\partial f}{\partial p}\frac{\partial p}{\partial \underline{\underline{\sigma}}} = 3\underline{\underline{\sigma}}^{\mathrm{D}} - \tfrac{M^2}{3}(2p - p_{\mathrm{c}})\,\underline{\underline{I}} \;, \tag{24}$$

$$m^2 = \underline{\underline{m}} : \underline{\underline{m}} = 6q^2 + \tfrac{M^4}{3}(2p - p_{\mathrm{c}})^2 \qquad , \quad \underline{\underline{n}} = \underline{\underline{m}}/m \;, \tag{25}$$

$$\frac{\partial \underline{\underline{m}}}{\partial \underline{\underline{\varepsilon}}_{\mathrm{e}}} = \left\{ \frac{\partial \underline{\underline{m}}}{\partial q}\frac{\partial q}{\partial \underline{\underline{\sigma}}} + \frac{\partial \underline{\underline{m}}}{\partial p}\frac{\partial p}{\partial \underline{\underline{\sigma}}} \right\} : \frac{\partial \underline{\underline{\sigma}}}{\partial \underline{\underline{\varepsilon}}_{\mathrm{e}}} = \left\{ 3\underline{\underline{P}} + \tfrac{2}{9}M^2\,\underline{\underline{I}} \otimes \underline{\underline{I}} \right\} : \underline{\underline{\underline{\underline{D}}}} \;, \tag{26}$$

$$\frac{\partial m^2}{\partial \underline{\underline{\varepsilon}}_{\mathrm{e}}} = \left\{ \frac{\partial m^2}{\partial q}\frac{\partial q}{\partial \underline{\underline{\sigma}}} + \frac{\partial m^2}{\partial p}\frac{\partial p}{\partial \underline{\underline{\sigma}}} \right\} : \frac{\partial \underline{\underline{\sigma}}}{\partial \underline{\underline{\varepsilon}}_{\mathrm{e}}} = \left\{ 18\underline{\underline{\sigma}}^{\mathrm{D}} - \tfrac{4}{9}M^4(2p - p_{\mathrm{c}})\,\underline{\underline{I}} \right\} : \underline{\underline{\underline{\underline{D}}}} \;, \tag{27}$$

$$\frac{\partial \underline{\underline{n}}}{\partial \Delta \underline{\underline{\varepsilon}}_{\mathrm{e}}} = \frac{1}{m}\left\{ \frac{\partial \underline{\underline{m}}}{\partial \underline{\underline{\varepsilon}}_{\mathrm{e}}} - \frac{1}{2}\,\underline{\underline{n}} \otimes \frac{1}{m}\frac{\partial m^2}{\partial \underline{\underline{\varepsilon}}_{\mathrm{e}}} \right\} : \frac{\partial \underline{\underline{\varepsilon}}_{\mathrm{e}}}{\partial \Delta \underline{\underline{\varepsilon}}_{\mathrm{e}}} \;, \tag{28}$$

$$\frac{\partial \underline{\underline{n}}}{\partial \Delta p_{\mathrm{c}}} = \frac{1}{m}\left\{ \frac{\partial \underline{\underline{m}}}{\partial p_{\mathrm{c}}} - \frac{1}{2}\,\underline{\underline{n}} \otimes \frac{1}{m}\frac{\partial m^2}{\partial p_{\mathrm{c}}} \right\} \frac{\partial p_{\mathrm{c}}}{\partial \Delta p_{\mathrm{c}}} = \frac{M^2}{3m}\left\{ \underline{\underline{I}} + M^2(2p - p_{\mathrm{c}})\,\underline{\underline{n}}/m \right\} \theta \;, \tag{29}$$

$$\frac{\partial f_{p_{\mathrm{c}}}}{\partial \underline{\underline{n}}} = \frac{f_{p_{\mathrm{c}}}}{\partial \Delta \varepsilon_{\mathrm{p}}^{\mathrm{V}}}\frac{\partial \Delta \varepsilon_{\mathrm{p}}^{\mathrm{V}}}{\partial \underline{\underline{n}}} = p_{\mathrm{c}}\vartheta\; \Delta\Lambda_p \underline{\underline{I}} \;. \tag{30}$$

The solution of System (20) can be accomplished based on the Karush Kuhn Tucker conditions with an elastic predictor and a plastic corrector step. This leads to a radial return mapping algorithm (also known as active set search). Alternatively, the case distinction can be avoided using the Fischer-Burmeister complementary condition [cf. e. g. 1, 2]. Both methods can be used in MFront [8, 9].

3.2 Numerical refinement and stabilization

It is recommended to normalize all residuals (20) to some similar order of magnitude, e. g. as strains. For this, equation (20b) can be divided by some characteristic value:

$$f_{\Lambda_p} = f/\hat{f} = \left\{ q^2 + M^2(p^2 - p\,p_{\mathrm{c}}) \right\} / (E\,p_{\mathrm{c0}}) \;. \tag{31}$$

Here $\hat{f} = E\,p_{\mathrm{c0}}$ was chosen with the elastic modulus and the initial value of the preconsolidation pressure. Of course, this has to be considered in the corresponding partial derivatives (22d–f). Instead of applying the same procedure to $f_{p_{\mathrm{c}}}$ it is advantageous to directly normalize the corresponding independent variable p_{c}. Then, the new reduced integration variable is

$$p_{\mathrm{c}}^r \coloneqq p_{\mathrm{c}}/\hat{p}_{\mathrm{c}} = p_{\mathrm{c}}/p_{\mathrm{c0}} \;. \tag{32}$$

Thus, the partial derivatives with respect to p_{c} have to be replaced as

$$\frac{\partial (*)}{\partial p_{\mathrm{c}}} \rightarrow \frac{\partial (*)}{\partial p_{\mathrm{c}}^r} = \frac{1}{\hat{p}_{\mathrm{c}}}\frac{\partial (*)}{\partial p_{\mathrm{c}}} \;. \tag{33}$$

Consequently, all integration variables $\underline{\underline{\varepsilon}}_{\mathrm{e}}, \Lambda_p, p_{\mathrm{c}}^r, \phi$ are dimensionless, strain-like variables, which improves the condition number of the set of equations.

In order to stabilize the numerical behaviour two more minor modifications are beneficial. The first one regards some (initial) state with zero stress. Then $f = 0$ is indicating

potential plastic loading, but plastic flow (11) is undetermined. To prevent this case, a small (ambient) pressure p_{amb} can be added to the hydrostatic pressure, i. e.

$$p \coloneqq -I_1(\underline{\underline{\sigma}})/3 + p_{\mathrm{amb}} \ . \tag{34}$$

Hence, a small initial elastic range is provided.

Another problem occurs in case of strong softening and dilatancy: $p_{\mathrm{c}} \to 0$ and the yield surface contracts until it degenerates to a single point such that the direction of plastic flow is undefined. In order to limit the decrease of p_{c} to some minimal pre-consolidation pressure $p_{\mathrm{c}}^{\mathrm{min}}$ the evolution equation (13) is modified to

$$\dot{p}_{\mathrm{c}} = -\dot{\varepsilon}_{\mathrm{p}}^{\mathrm{V}} \vartheta(e) \ (p_{\mathrm{c}} - p_{\mathrm{c}}^{\mathrm{min}}) \quad \text{with} \quad p_{\mathrm{c}}\big|_{t=0} = p_{\mathrm{c0}} \ , \tag{35}$$

where the normalization from above can be applied again. A reasonably small value for $p_{\mathrm{c}}^{\mathrm{min}}$ can be, e. g., the ambient atmospheric pressure. The modifications need to be considered in Eq. (20c) and its derivatives.

3.3 Semi-explicit solution scheme

The number of equations in System (20) can be reduced exploiting the minor influence of the porosity in a given time step. Since ϕ usually does not significantly change during the strain increment, it can be updated explicitly at the end of the time step [4]. Exploiting formula (42) yields

$$^{k+1}\phi = 1 - \ (1 - {}^{k}\phi) \exp(-\Delta\varepsilon^{\mathrm{V}}) \quad \text{or} \tag{36}$$

$$^{k+1}\phi = {}^{k}\phi + \Delta\phi \quad \text{with} \quad \Delta\phi = (1 - {}^{k}\phi) \left[1 - \exp(-\Delta\varepsilon^{\mathrm{V}})\right] \ . \tag{37}$$

Thus, the residual equation (20d) and the corresponding derivatives can be omitted. The pore number follows directly from the new porosity value using the relation

$$1 + {}^{k+1}e = \frac{1}{1 - {}^{k+1}\phi} \ . \tag{38}$$

4 Implementation into MFront

For the *MFront* implementation the domain specific language (DSL) `Implicit` was used, cf. [8, 12]. The coupling to OpenGeoSys [10, 3] is done using MGIS [9]. The implementation is part of the *OpenGeoSys* source code, cf. `https://gitlab.opengeosys.org`.

In the preamble of the *MFront* code the parameters are specified and integration variables are declared. Note that a *state variable* is a persistent variable and an integration variable, whereas an *auxiliary state variable* is also persistent but no integration variable.

```
// environmental parameters (default values)
@Parameter stress pamb = 1e+3; //Pa
@PhysicalBounds pamb in [0:*[;
pamb.setEntryName("AmbientPressure");
```

```
// material parameters
@MaterialProperty stress young;
@PhysicalBounds young in [0:*[;
young.setGlossaryName("YoungModulus");
...
@StateVariable real lp;
lp.setGlossaryName("EquivalentPlasticStrain");
@IntegrationVariable strain rpc;
@AuxiliaryStateVariable stress pc;
pc.setEntryName("PreConsolidationPressure");
@AuxiliaryStateVariable real phi;
phi.setGlossaryName("Porosity");
...
```

The semi-explicit solution scheme is then implemented with three basic steps:

```
@InitLocalVariables{
  //elastic predictor step
}
@Integrator{
  //plastic corrector step
}
@UpdateAuxiliaryStateVariables{
  //explicit porosity update
}
```

5 Numerical studies

5.1 Consolidated plane strain simple shear test using mtest

MFront provides the tool *mtest* for testing the implemented material behaviour at a single material point (integration point), see [8]. For this, non-monotonic loading sequences can be prescribed in terms of stress and strain trajectories.

In order to test the consolidation behaviour, plane strain simple shear tests were conducted with the same initial state but three different loading trajectories. To be precise, first the hydrostatic pressure p was increased until $0.25\,p_{c0}, 0.5\,p_{c0}$ or $0.75\,p_{c0}$. This results in the so-called overconsolidation ratios (OCR) of $4, 2, 4/3$. From this hydrostatic stress state, shear is applied up to the strain $\varepsilon_{xy} = 0.01$.

Table 1: Material parameters for the basic modified Cam clay model

E / Pa	ν	M	λ	κ	ϕ_0	p_{c0} / Pa	p_{amb} / Pa
$150 \cdot 10^9$	0.3	1.5	$7.7 \cdot 10^{-3}$	$6.6 \cdot 10^{-4}$	0.44	$30 \cdot 10^6$	$0 \cdot 10^3$

The material parameters are given in Table 1. It should be noted that only the difference $\lambda - \kappa$ plays a role in the basic model with *constant* elastic parameters. Considering the OCR, there are three different cases (cf. Figure 1):

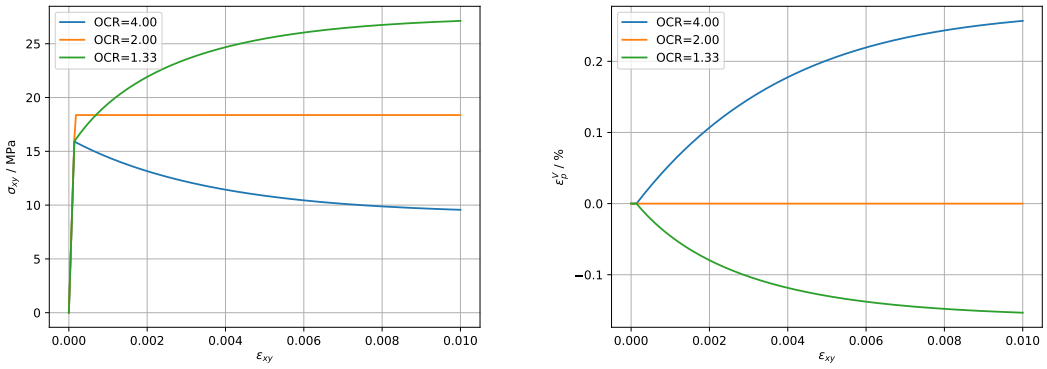

Figure 1: Consolidated shear test for three typical OCR values: $\varepsilon_{\mathrm{p}}^{\mathrm{V}} > 0$ causes softening, whereas $\varepsilon_{\mathrm{p}}^{\mathrm{V}} < 0$ (compaction) results in hardening.

For OCR > 2 the shearing is accompanied by a plastic expansion (dilatancy) with $\varepsilon_{\mathrm{p}}^{\mathrm{V}} > 0$, which causes softening until the critical state is reached.

For OCR $= 2$ shearing until yield leads directly to the critical state. Considering the state of the soil (porosity, stress, volume) this is a natural asymptotic state. Further shearing does not alter that state anymore. Hence, there is ideal plastic behaviour.

For OCR < 2 the shearing is accompanied by a plastic compaction (contractant flow, consolidation) with $\varepsilon_{\mathrm{p}}^{\mathrm{V}} < 0$, which causes hardening until the critical state is reached.

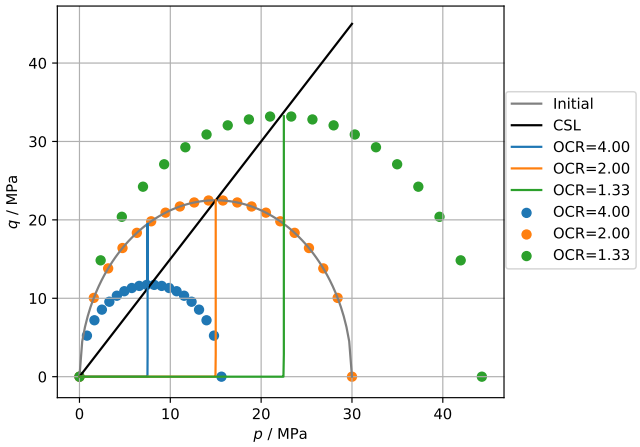

Figure 2: Consolidated shear test for 3 typical OCR values: depicted are the different stress trajectories, the critical state line (CSL) and the final yield surfaces.

The stress trajectories, and the final yield surfaces are illustrated in the p, q-space together with the initial yield surface and the critical state line (CSL).

Now, the same consolidated shear loading is applied, but there are two different initial states: a high value of the initial pre-consolidation pressure p_{c0} resembles a heavily pre-consolidated, compacted (dense) soil material, whereas a low value of p_{c0} resembles a loosened initial state.

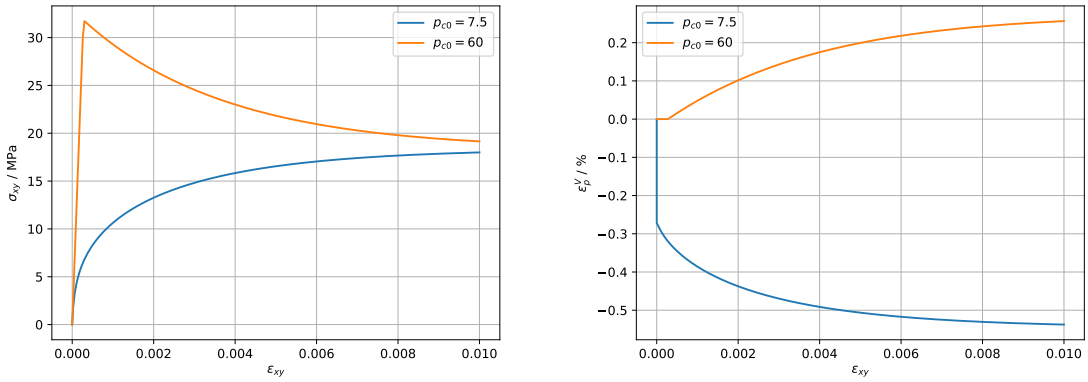

Figure 3: Consolidated shear test for two different initial pre-consolidation pressures.

As can be seen in Figure 3 and 4 the materials thrive to the same (asymptotic) critical state, since the CSL is identical. However, this is either accomplished by hardening (contraction) or softening (dilatancy).

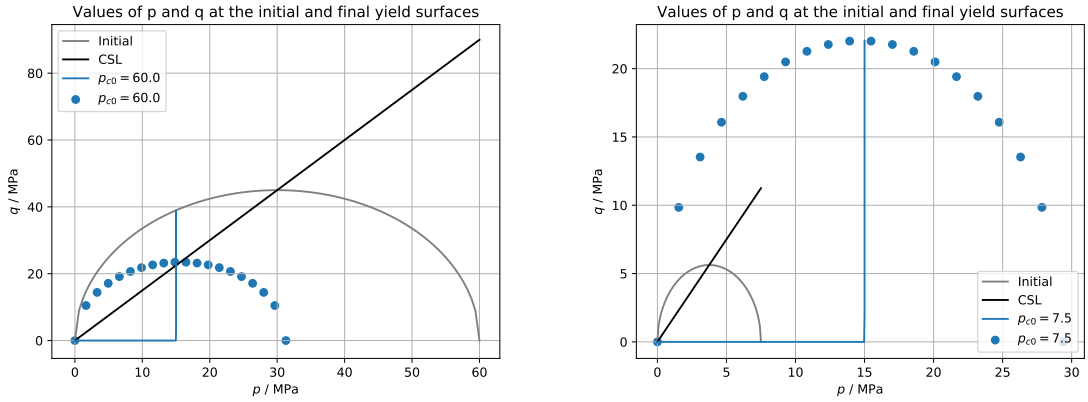

Figure 4: Consolidated shear test for two different initial pre-consolidation pressures: the CSL and the final state including the final yield surface are equal.

5.2 Plane strain simple shear test with one FE using OpenGeoSys

As a next step the shear test from the previous section was repeated using *OpenGeoSys*, but without consolidation phase. A unit square domain was meshed with only one finite element. At the boundaries (top, bottom, left, right) Dirichlet boundary conditions (BCs) were prescribed. The top boundary was loaded by a linear ramp from time 0 to 1 s. The material parameters were taken from Table 1 with only one difference: As the test has no pre-consolidation phase, it is starting from zero stress and due to the reasons explained in subsection 3.2 some small initial ambient pressure $p_{\text{amb}} = 1 \cdot 10^3$ Pa was added.[3]

Test	BC left	BC right	BC top	BC bottom	behaviour
Shear xy	free	free	$u_x = -0.05t$	$u_x = u_y = 0$	no convergence
Shear xy	free	free	$u_x = -0.05t, u_y = 0$	$u_x = u_y = 0$	convergence

Table 2: Convergence behaviour for different shear loadings and BCs.

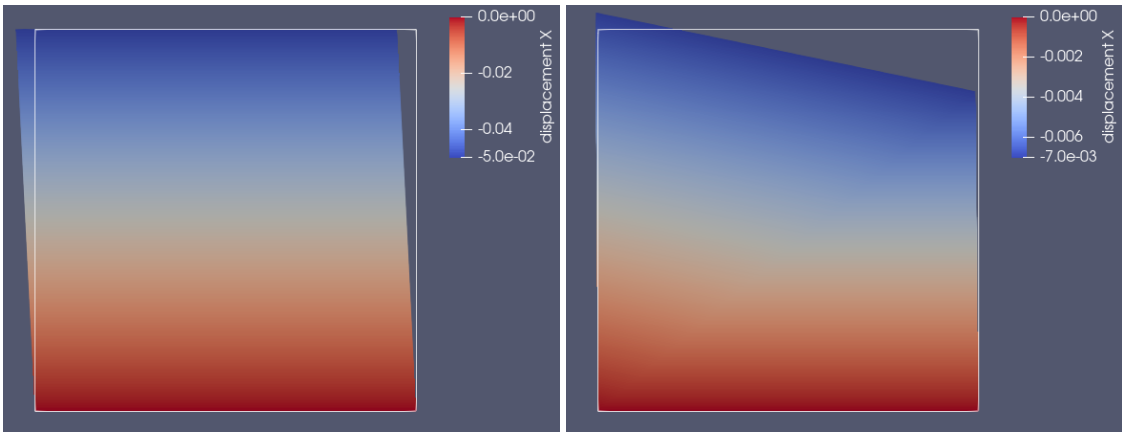

Figure 5: Test results for different BCs according to Table 2: the top boundary is either confined (*left*) or free (*right*).

In order to have true simple shear the top BC $u_y = 0$ has to be applied. Else there is a tilting effect, and the deformation consists of shear and bending. As this is related to some parts with dominant tension stresses, convergence cannot be achieved with the Cam clay model (cf. next section). Note also that for pure shear $\varepsilon^{\text{V}} = 0$ and the volume and porosity thus remain constant.

5.3 Plane strain simple biaxial test with one FE using OpenGeoSys

It must be noted that the Cam clay model is primarily intended to capture the shear behaviour of soil materials *without* cohesion. Hence, the uniaxial stress states with free

[3] If the test is stress-controlled and the material is initially on the critical state with zero stress, this causes an infinite strain increment and no convergence can be expected.

boundaries cannot be sustained just as these states cannot be reached in reality. As an example, uniaxial tension causes pronounced lateral stretching due to plastic volume increase (dilatancy). The application of some minimal pre-consolidation pressure can help to stabilize the simulation, but convergence cannot be expected in general.

Still, the biaxial tension/compression behaviour can be simulated to a certain degree. The Table 3 shows under which conditions convergence can be expected. In the converged cases a homogeneous solution was obtained as expected.

Test	BC left	BC right	BC top	BC bottom	convergence
Uniax. compr. y	$u_x = 0$	free	$u_y = -0.05t$	$u_y = 0$	no
Uniax. tension y	$u_x = 0$	free	$u_y = +0.05t$	$u_y = 0$	no
Biaxial compr. x, y	$u_x = 0$	$u_x = -0.05t$	$u_y = -0.05t$	$u_y = 0$	yes
Biaxial tension x, y	$u_x = 0$	$u_x = +0.05t$	$u_y = +0.05t$	$u_y = 0$	(yes)
Biaxial mixed x, y	$u_x = 0$	$u_x = +0.05t$	$u_y = -0.05t$	$u_y = 0$	yes
Biaxial mixed x, y	$u_x = 0$	$u_x = -0.05t$	$u_y = +0.05t$	$u_y = 0$	yes

Table 3: Convergence behaviour for different biaxial loadings and BCs

It is interesting to note that the biaxial tension test can be simulated with the Cam clay model. In order to achieve convergence the drop of the pre-consolidation pressure has to be limited. For this, either the value of the parameter difference $\lambda - \kappa$ is increased or some minimal value $p_c^{\min}$ has to be ensured according to Eq. (35).

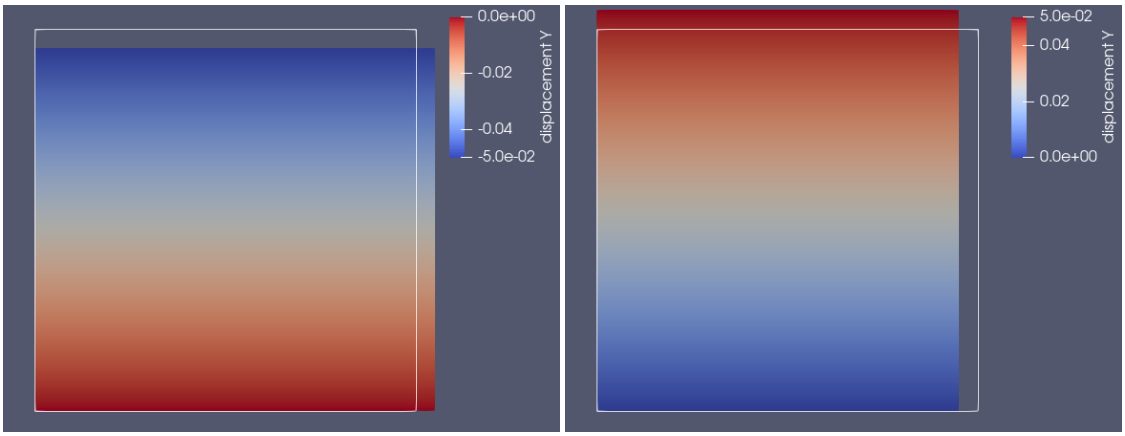

Figure 6: Biaxial test results for different BCs: shown are the mixed cases from Table 3.

5.4 Axially-symmetric triaxial compression test

As a benchmark to existing results an axially-symmetric triaxial compression test was performed. For this, a cylindrical domain of height 100 m and radius 25 m is meshed with 100×25 finite elements. At the left and bottom boundaries symmetry BCs of Dirichlet type are prescribed. The top and right boundaries are loaded by prescribing an axial

and a confining pressure p_{con}, respectively. The loading consists of two stages, similar to subsection 5.1: iI) a linear ramp until a hydrostatic stress state with $p = p_{\text{con}} = 200\,\text{kPa}$ is reached (with an OCR=1) and ii) a further increase of the axial pressure while the confining pressure p_{con} is held constant. As the simulation time is irrelevant it is again set to 1 s. The material parameters are taken from Table 4.

Table 4: Material parameters for the basic modified Cam clay model

E / Pa	ν	M	λ	κ	ϕ_0	p_{c0} / Pa	p_{amb} / Pa
$52 \cdot 10^6$	0.3	1.2	$7.7{\cdot}10^{-2}$	$6.6{\cdot}10^{-3}$	0.44	$200 \cdot 10^3$	$1 \cdot 10^3$

The material and loading parameters were chosen such that the stress trajectory approaches the CSL from the right but does not meet it (cf. Figure 9). When this happens there will be zero resistance to plastic flow causing an infinite strain increment in the stress-controlled test and no convergence can be expected. The tendency can already be seen in Figure 8 with the steep increase of the equivalent plastic strain.

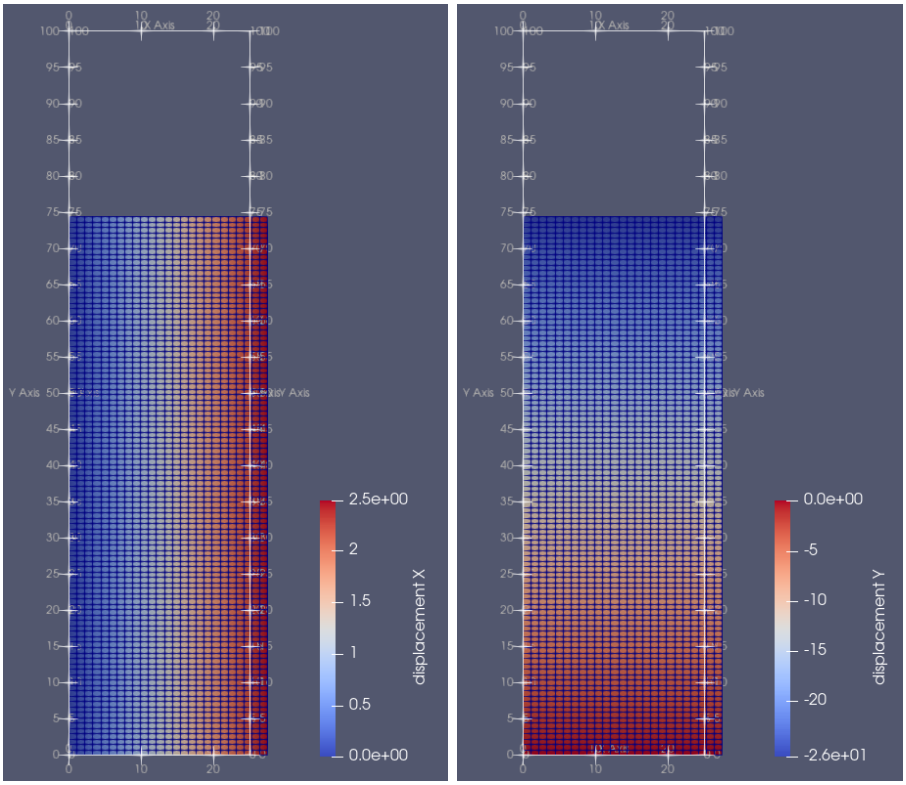

Figure 7: Triaxial benchmark results: shown are the displacement coefficients in the radial (here x) and the vertical (here y) direction.

The curve of the pre-consolidation pressure (cf. Figure 8 left) shows monotonic hardening related to the plastic compaction (cf. Figure 8 right).

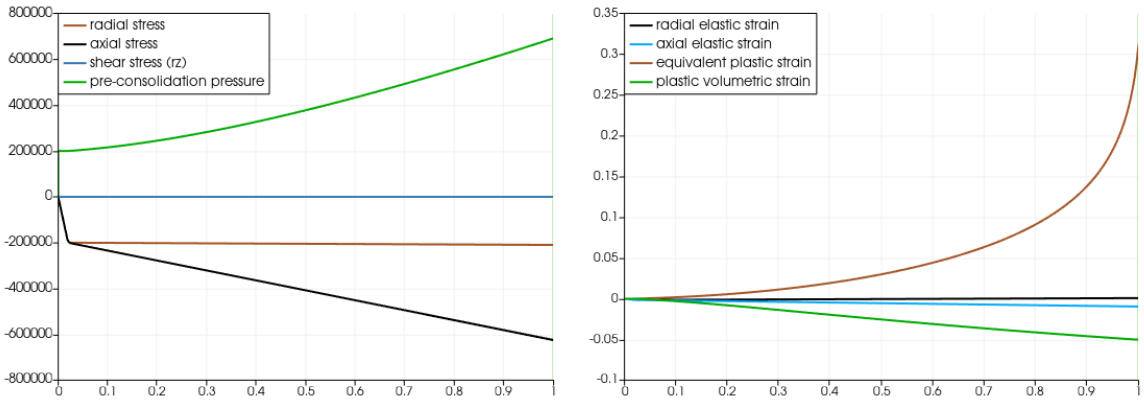

Figure 8: Triaxial benchmark results: shown is the evolution of stress (*left*, unit Pa) and strain measures (*right*) at some arbitrary integration point.

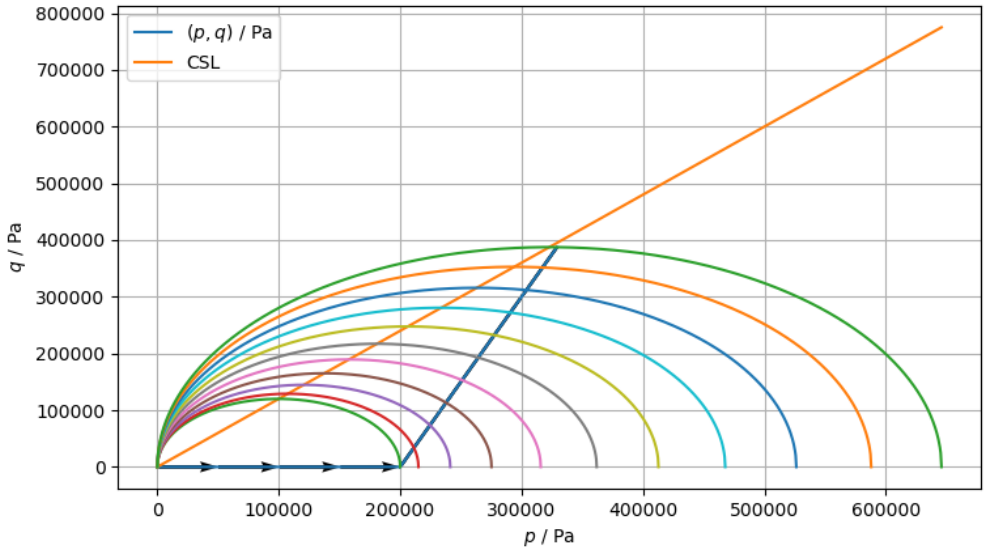

Figure 9: Triaxial benchmark results: depicted is the stress trajectory and the evolving yield surface as well as the CSL.

In order to check the accuracy of the numerical results, they were compared to an analytical solution [13] for proportional loading. For this, the straight stress path from $(q = 0, p = p_{\text{con}})$ until the final state is considered (cf. Figure 9). The plot of the von-Mises stress over the corresponding equivalent strain defined by $\varepsilon_{\text{q}}^2 = \frac{2}{3}\,\underline{\underline{\varepsilon}}^{\text{D}} \cdot\cdot\, \underline{\underline{\varepsilon}}^{\text{D}}$ shows

accurate agreement between numerical and analytical solution (cf. also the appendix). Minor deviations might arise from the assumption (16) [13], whereas a constant bulk modulus according to Eq. (17) was applied here. Considering the radial and circumferential strains another peculiarity is found (cf. Figure 10): The initial plastic compaction causes lateral (i. e. radial and circumferential) contraction. However, with increasing axial compression this necessarily turns into expansion. Note also that for this *numerical* test the magnitude of the strains is beyond the scope of the linear strain measure.

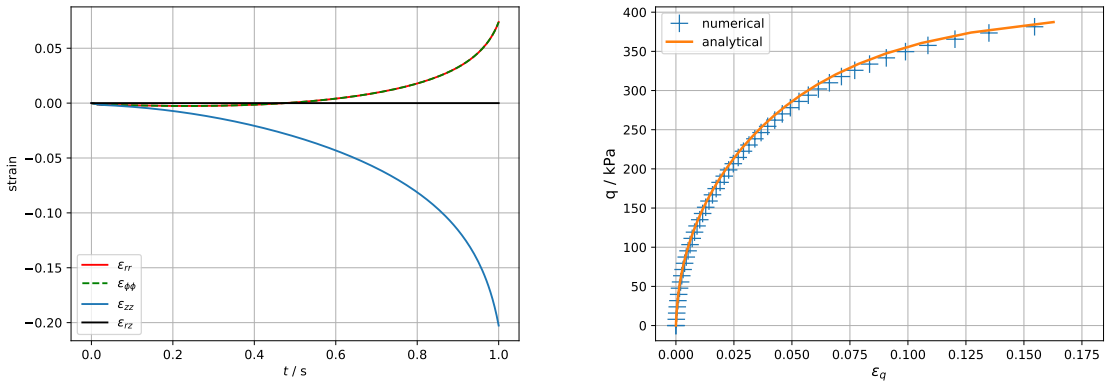

Figure 10: Triaxial benchmark results: depicted are the strain trajectories (*left*) and a comparison between analytical and numerical solution (*right*).

As an alternative the test can, of course, also be conducted displacement-controlled. However, in doing so it was found that the homogeneous solution becomes unstable and strain localization occurs at the top of the domain. Apparently, at some integration points softening sets in even though the homogeneous solution only shows monotonic hardening. Varying the mesh size and topology, convergence could be achieved in some cases, indicating a strong mesh dependency.

6 Concluding remarks

The presented Cam clay material model has a simple structure, but can capture several characteristic phenomena of soil materials very well. However, it must be considered with caution when applied to realistic finite element simulations. The major limitations have two origins: first, the missing cohesion and second, the dilatant/softening part of the captured material behaviour. The provided numerical refinements can stabilize this only to a limited degree. It seems that the softening can cause a pronounced strain localization, which requires special strategies for regularization of the underlying ill-posed mathematical problem [cf. e. g. 11]. In order to include finite cohesion different modifications of the Cam clay model have been proposed [cf. e. g. 7]. Finally, mechanical loading in the vicinity of the critical state can easily cause large deformations, a finite strain formulation should be considered in the future [cf. e. g. 5, 6].

Appendix

Numerical convergence behavior of the modified Cam clay implementation

In order to check the convergence rate of the Cam clay implementation the consolidated shear test from Section 5.1 was considered again. The parameters were taken from Table 1. The hydrostatic pressure p was increased until $0.66\,p_{c0}$ resulting in an OCR of 1.5. From this hydrostatic stress state, shear is applied up to the strain $\varepsilon_{xy} = 5 \cdot 10^{-4}$ within 20 time steps.

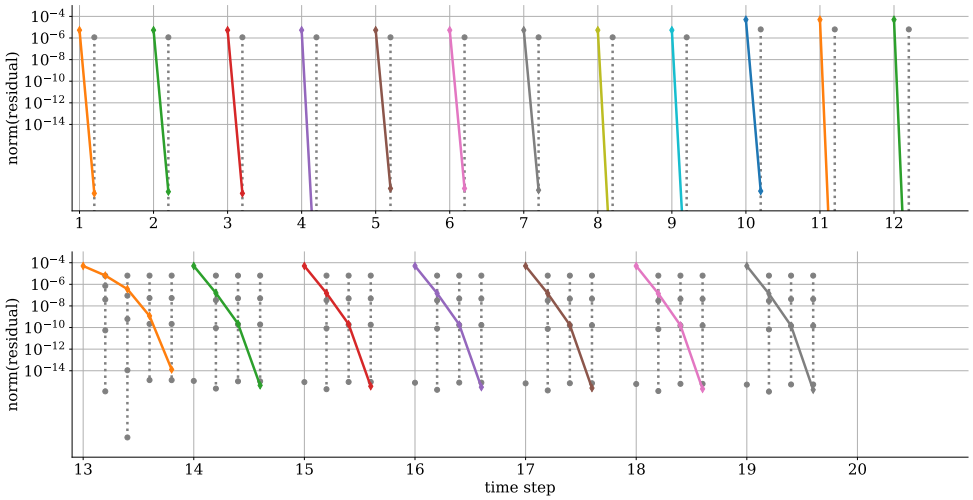

Figure 11: Convergence plot: depicted is the norm of the residuals from the global iteration (colored) and the local iteration (grey) using the modified Cam clay *MFront* implementation and *mtest*. Within the first 12 steps the behavior is purely elastic (*top*), followed by contractant plastic flow (*bottom*).

As can be seen in Figure 11, convergence is achieved in one step in the elastic stage (*top*). In the plastic stage (*bottom*), the typical acceleration of convergence when approaching the solution is observed (asymptotic quadratic convergence). However, the convergence depends on the plastic flow behavior dictated by the parameters M, λ-κ and p_{c0} and can reduce to super-linear (order $\in [1, 2]$).

Orthotropic modified Cam clay model implementation

The implementation of the modified Cam clay model can be extended to orthotropic elastic behavior using the so-called standard bricks within *MFront*. Thus just one line of code need to be added:

```
@Brick StandardElasticity;
@OrthotropicBehaviour<Pipe>;
```

As a consequence the nine independent constants of orthotropic elasticity are already declared.

```
// material parameters
// Note: YoungModulus and PoissonRatio defined as parameters
// Note: Glossary names are already given; entry names are newly defined
@MaterialProperty real M;
@PhysicalBounds M in [0:*[;
M.setEntryName("CriticalStateLineSlope");
...
```

However, from the physical point of view it might be more realistic to consider the anisotropy both for the elastic and plastic behavior.

Analytical expressions for porosity and pre-consolidation pressure evolution

Given is the evolution equation for the porosity:

$$\dot{\phi} - \phi \operatorname{div}(\dot{\underline{u}}) = \operatorname{tr}(\dot{\underline{\underline{\varepsilon}}}) \quad \text{with} \quad \varepsilon^{\mathrm{V}} = \operatorname{tr}(\underline{\underline{\varepsilon}}) \ . \tag{39}$$

Exploiting $\operatorname{div}(\dot{\underline{u}}) \equiv \operatorname{tr}(\dot{\underline{\underline{\varepsilon}}})$ and separating the variables yields the form

$$\frac{\mathrm{d}\phi}{1-\phi} = \mathrm{d}\varepsilon^{\mathrm{V}} \ . \tag{40}$$

Integration over some time increment Δt with $\phi(t) = {}^{k}\phi$ and $\phi(t+\Delta t) = {}^{k+1}\phi$ as well as $\Delta\varepsilon^{\mathrm{V}} = {}^{k+1}\varepsilon^{\mathrm{V}} - {}^{k}\varepsilon^{\mathrm{V}}$ as the volumetric strain increment, i. e.

$$\int_{{}^{k}\phi}^{{}^{k+1}\phi} \frac{\mathrm{d}\phi}{1-\phi} = \int_{{}^{k}\varepsilon^{\mathrm{V}}}^{{}^{k+1}\varepsilon^{\mathrm{V}}} \mathrm{d}\varepsilon^{\mathrm{V}} \ . \tag{41}$$

then results in the incremental solution

$$1 - {}^{k+1}\phi = (1 - {}^{k}\phi) \exp(-\Delta\varepsilon^{\mathrm{V}}) \ . \tag{42}$$

Integration over the whole process time span with the initial values $\phi(t=0) = {}^{0}\phi$ and $\varepsilon^{\mathrm{V}}(t=0) = 0$ results in

$$1 - \phi = (1 - {}^{0}\phi) \exp(-\varepsilon^{\mathrm{V}}) \ . \tag{43}$$

Combining (43) with (13) finally yields the evolution of the pre-consolidation pressure:

$$\dot{p}_{\mathrm{c}} = -\frac{\dot{\varepsilon}_{\mathrm{p}}^{\mathrm{V}} p_{\mathrm{c}}}{(\lambda - \kappa)(1 - {}^{0}\phi) \exp(-\varepsilon^{\mathrm{V}})} \ . \tag{44}$$

Analytical solution of the Cam clay model for proportional loading

A straight stress path from $(p, q) = (0, p_{c0})$ until the final state $(p, q) = (387387, 330129)$ Pa is considered:

$$q = k\,(p - p_{c0})\ . \tag{45}$$

The analytical solution [13] for the corresponding equivalent strain $\varepsilon_q^2 = \frac{2}{3}\ \underline{\underline{\varepsilon}}^D \cdot\cdot\ \underline{\underline{\varepsilon}}^D$ reads

$$\varepsilon_q = \varepsilon_q^e + \varepsilon_q^p \tag{46}$$

and to be precise, using the abbreviations $C = (\lambda\text{-}\kappa)$ and $\alpha = 3(1-2\nu)/(2(1+\nu))$ it is

$$(1+e_0)\,\varepsilon_q^e = \ln\left[\left(1 - \frac{q}{kp}\right)^{\frac{2Ck}{k^2-M^2} - \frac{\kappa k}{3\alpha}}\right]\ , \tag{47}$$

$$(1+e_0)\,\varepsilon_q^p = \ln\left[\left(1 - \frac{q}{Mp}\right)^{\frac{Ck}{M(M-k)}} \cdot \left(1 + \frac{q}{Mp}\right)^{\frac{Ck}{M(M+k)}}\right] - 2\frac{C}{M}\arctan\left(\frac{q}{Mp}\right)\ . \tag{48}$$

References

[1] M. J. Ashrafi et al. "Theoretical and numerical modeling of dense and porous shape memory alloys accounting for coupling effects of plasticity and transformation". In: *International Journal of Solids and Structures* 88-89 (2016), pp. 248–262. ISSN: 00207683. DOI: 10.1016/j.ijsolstr.2016.03.003. URL: http://dx.doi.org/10.1016/j.ijsolstr.2016.03.003.

[2] T. Bartel et al. "Investigations on enhanced Fischer–Burmeister NCP functions: application to a rate-dependent model for ferroelectrics". In: *Archive of Applied Mechanics* 89.6 (2019), pp. 995–1010. ISSN: 14320681. DOI: 10.1007/s00419-018-1466-7. URL: https://doi.org/10.1007/s00419-018-1466-7.

[3] Lars Bilke et al. "Development of Open-Source Porous Media Simulators: Principles and Experiences". In: *Transport in Porous Media* 130.1 (Oct. 2019), pp. 337–361. ISSN: 0169-3913. DOI: 10.1007/s11242-019-01310-1. URL: http://link.springer.com/10.1007/s11242-019-01310-1.

[4] Ronaldo I. Borja and Seung R. Lee. "Cam-Clay plasticity, Part 1: Implicit integration of elasto-plastic constitutive relations". In: *Computer Methods in Applied Mechanics and Engineering* 78.1 (1990), pp. 49–72. ISSN: 00457825. DOI: 10.1016/0045-7825(90)90152-C.

[5] Ronaldo I. Borja and Claudio Tamagnini. "Cam-Clay plasticity: Part III: Extension of the infinitesimal model to include finite strains". In: *Computer Methods in Applied Mechanics and Engineering* 155.1-2 (1998), pp. 73–95. ISSN: 00457825. DOI: 10.1016/S0045-7825(97)00141-2.

[6] C. Callari, F. Auricchio, and E. Sacco. "A finite-strain cam-clay model in the framework of multiplicative elasto-plasticity". In: *International Journal of Plasticity* 14.12 (1998), pp. 1155–1187. ISSN: 07496419. DOI: 10.1016/S0749-6419(98)00050-3.

[7] J. Gaume et al. “Dynamic anticrack propagation in snow”. In: *Nature Communications* 9.1 (2018). ISSN: 20411723. DOI: 10.1038/s41467-018-05181-w. URL: http://dx.doi.org/10.1038/s41467-018-05181-w.

[8] Thomas Helfer et al. “Introducing the open-source mfront code generator: Application to mechanical behaviours and material knowledge management within the PLEIADES fuel element modelling platform”. In: *Computers & Mathematics with Applications* 70.5 (Sept. 2015), pp. 994–1023. ISSN: 08981221. DOI: 10.1016/j.camwa.2015.06.027. URL: https://linkinghub.elsevier.com/retrieve/pii/S0898122115003132.

[9] Thomas Helfer et al. “The MFrontGenericInterfaceSupport project”. In: *Journal of Open Source Software* 5.48 (Apr. 2020), p. 2003. ISSN: 2475-9066. DOI: 10.21105/joss.02003. URL: https://joss.theoj.org/papers/10.21105/joss.02003.

[10] O Kolditz et al. “OpenGeoSys: an open-source initiative for numerical simulation of thermo-hydro-mechanical/chemical (THM/C) processes in porous media”. In: *Environmental Earth Sciences* 67.2 (2012), pp. 589–599.

[11] Miguel A. Mánica et al. “Nonlocal plasticity modelling of strain localisation in stiff clays”. In: *Computers and Geotechnics* 103.July (2018), pp. 138–150. ISSN: 18737633. DOI: 10.1016/j.compgeo.2018.07.008. URL: https://doi.org/10.1016/j.compgeo.2018.07.008.

[12] Gentien Marois et al. “Invariant-based implementation of the Mohr-Coulomb elasto-plastic model in OpenGeoSys using MFront”. In: April (2020). DOI: 10.13140/RG.2.2.34335.10403.

[13] Dunja Perić. “Analytical solutions for a three-invariant Cam clay model subjected to drained loading histories”. In: *International Journal for Numerical and Analytical Methods in Geomechanics* 30.5 (2006), pp. 363–387. ISSN: 03639061. DOI: 10.1002/nag.482.